Microbiome

METHODOLOGY

Open Access

pH-FISH: coupled microscale analysis of microbial identity and acid–base metabolism in complex biofilm samples

Yumi Chokyu Del Rey[1*], Katharina Kitzinger[2], Marie Braad Lund[3], Andreas Schramm[3], Rikke Louise Meyer[3,4], Michael Wagner[2,5,6] and Sebastian Schlafer[1*]

Abstract

Background Correlative structural and chemical imaging of biofilms allows for the combined analysis of microbial identity and metabolism at the microscale. Here, we developed pH-FISH, a method that combines pH ratiometry with fluorescence in situ hybridization (FISH) in structurally intact biofilms for the coupled investigation of microbial acid metabolism and biofilm composition. Careful biofilm handling and modified sample preparation procedures for FISH allowed preservation of the three-dimensional biofilm structure throughout all processing and imaging steps. We then employed pH-FISH to investigate the relationship between local biofilm pH and the distribution of acid-producing (streptococci) and acid-consuming (*Veillonella* spp.) bacteria in dental biofilms from healthy subjects and caries-active patients.

Results The relative abundance of streptococci correlated with low biofilm pH at the field-of-view level, while the opposite trend was observed for *Veillonella* spp. These results suggest that clusters of streptococci contribute to the formation of acidic pockets inside dental biofilms, whereas *Veillonella* spp. may have a protective role against biofilm acidification.

Conclusions pH-FISH combines microscale mapping of biofilm pH in real time with structural imaging of the local microbial architecture, and is a powerful method to explore the interplay between biofilm composition and metabolism in complex biological systems.

Keywords Fluorescence in situ hybridization, pH ratiometry, Confocal laser scanning microscopy, Microenvironments, Biofilms, Dental biofilms

*Correspondence:
Yumi Chokyu Del Rey
yumi@dent.au.dk
Sebastian Schlafer
sebastians@dent.au.dk
[1] Section for Oral Ecology, Cariology, Department of Dentistry and Oral Health, Aarhus University, Vennelyst Boulevard 9, 8000 Aarhus C, Denmark
[2] Centre for Microbiology and Environmental Systems Science, University of Vienna, Djerassiplatz 1, 1030 Vienna, Austria
[3] Section for Microbiology, Department of Biology, Aarhus University, Ny Munkegade 116, 8000 Aarhus C, Denmark
[4] Interdisciplinary Nanoscience Center, Aarhus University, Gustav Wieds Vej 14, 8000 Aarhus C, Denmark
[5] Center for Microbial Communities, Department of Chemistry and Bioscience, Aalborg University, Aalborg, Denmark
[6] The Comammox Research Platform, University of Vienna, Vienna, Austria

Background

Fluorescence in situ hybridization (FISH) with rRNA-targeted probes is a powerful molecular method that enables the direct identification, quantification, and localization of microorganisms within complex microbial communities without prior cultivation [1]. FISH has been widely used to study the abundance and spatial arrangement of microorganisms within biofilms and thereby contributed greatly to revealing their structural organization [2–5]. In complex microbial systems, however, it is equally important to trace the metabolic activities of microorganisms in situ. Multispecies biofilms exhibit highly heterogeneous chemical profiles at the microscale, with steep spatiotemporal gradients of solutes like oxygen or protons that are driven by the metabolic activity of specific microorganisms. Dental biofilm is a prime example of a highly complex microbial community, where biofilm pH varies substantially over a small spatial scale of a few hundred micrometers [6–8]. These pH differences have strong implications for the development of dental caries, as localized low-pH areas within dental biofilms are linked to the onset and progression of the disease [9, 10].

Several methodologic approaches have been developed to allow for a simultaneous analysis of microbial identity and metabolism. Microautoradiography (MAR) [11], nano-scale and conventional secondary ion mass spectrometry (SIMS) [12, 13], stable-isotope Raman spectroscopy [14, 15], and stimulated Raman spectroscopy (SRS) [16] have all been combined with FISH to provide insight into the metabolic processes carried out by specific microorganisms in mixed communities. These methods rely on the detection of radioactive or stable isotopically labeled substrates assimilated by the cells during growth, and they therefore do not provide a real-time analysis of the microbial metabolism, or its effect on microscale chemical gradients. The direct measurement of temporal chemical gradients within biofilms has been performed with a combination of FISH and microsensors [17–19]. The insertion of a microsensor, however, perturbs the biofilm structure mechanically, and due to the fragility of the employed electrodes, only vertical chemical profiles can be recorded [20].

In contrast to microsensors, confocal microscopy-based pH ratiometry allows for real-time monitoring of extracellular biofilm pH in all three dimensions without mechanically disturbing the biofilm [21, 22]. pH ratiometry exploits the proton-dependent shifts in excitation or emission of a ratiometric, pH-sensitive dye to determine fluorescence intensity ratios that are directly correlated to biofilm pH and independent of the dye concentration or photobleaching [23]. In this study, we aimed to combine pH ratiometry with FISH (pH-FISH) for the coupled investigation of microbial acid metabolism and biofilm composition at the microscale. As a proof-of-principle, pH-FISH was employed to visualize extracellular pH gradients and the spatial distribution of the predominant bacteria in dental biofilms from healthy subjects and caries-active patients.

Methods

Study participants

Three healthy participants and three caries-active patients were enrolled in this study. Detailed participant information and eligibility criteria are provided in Supplemental Material 1. The study was conducted in accordance with the Declaration of Helsinki and its amendments and approved by the Ethical Committee of Region Midtjylland (case no. 1–10-72–178-18). Written informed consent was obtained from all participants.

Fabrication of intraoral splints for biofilm collection

Digital impressions of the upper and lower jaws were obtained for each patient with an intraoral scanner (TRIOS4; 3Shape, Copenhagen, Denmark) and used to produce individual lower-jaw splints, as described in detail elsewhere [24]. Briefly, the splint structure consisted of a half-round metallic bar (1.75 × 1.38 mm), manufactured to adapt to the lingual surfaces of all inferior teeth, the distal surface of the most posterior tooth in each quadrant, and the buccal aspect of molars and premolars. 3-D-printed inserts with five standardized slots (3 mm recession depth) for biofilm carriers were produced by vat photopolymerization (Asiga MAX UV; Alexandria, Australia) and attached to the retention areas on each side of the metallic bars using light-cured acrylic material (Triad VLC Gel; Dentsply Sirona, Charlotte, NY) (Fig. 1B). Custom-made non-fluorescent glass slabs (4 × 4 × 1.5 mm; surface roughness, 1200 grit, mimicking the human enamel surface; Menzel, Braunschweig, Germany) were used as carriers for in situ biofilm formation. Prior to insertion into the splints, nine fields of view (FOVs) were marked on each glass slab using a laser microdissection microscope (Leica LMD7000; Leica Microsystems, Wetzlar, Germany) to standardize the imaged areas of the biofilms and facilitate re-imaging of the FOVs. The marks were placed at × 20 magnification with the following laser settings: power 60, aperture 30, speed 10, balance 15, head current 70%, and pulse frequency 500. The FOVs were 150 × 150 µm in size, 500 µm apart from each other, and at least 1200 µm away from the corners of the glass slab (Fig. 1A).

Biofilm growth and collection

For in situ biofilm formation, marked glass slabs were inserted into the slots of the 3-D-printed inserts of the

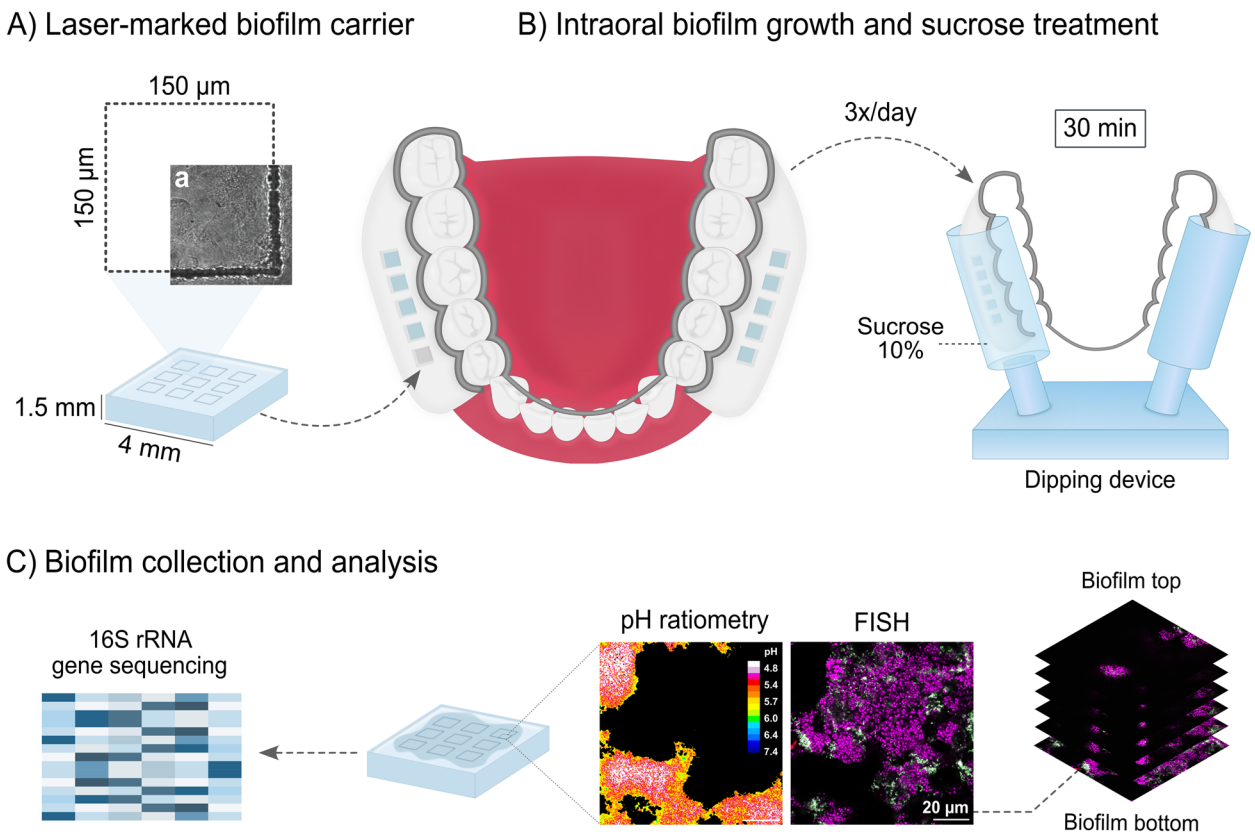

Fig. 1 Summary of the study design. **A** Biofilm carriers (glass slabs 1.5 × 4 × 4 mm) were laser-marked in nine fields of view (FOVs; 150 × 150 µm) using a laser microdissection microscope. The bottom right corner of the laser-marked FOVs (a: transmitted light micrograph) was used as a reference to standardize the imaged biofilm areas. **B** Individual lower-jaw splints with 3-D-printed inserts were fabricated to carry the laser-marked glass slabs during intraoral biofilm growth. All participants used the intraoral splint continuously for 2 days and treated the growing biofilms 3 ×/day by immersing both sides of the splint into a sucrose solution (10% w/v) for 30 min at room temperature. **C** After collection, the biofilms were either subjected to 16S rRNA gene amplicon sequencing (left) or pH-FISH (right). Biofilm pH was monitored in the laser-marked FOVs using pH ratiometry with the dye C-SNARF-4. Thereafter, the biofilms were embedded/fixed, dehydrated, permeabilized, and hybridized. FISH images were acquired in the same FOVs visualized by pH ratiometry and as 6-sliced z-stacks spanning the height of the biofilm

lower-jaw splints. The participants were instructed to wear the intraoral splints with the biofilm carriers for 48 h, and to dip the splints into 10% (w/v) sucrose solution 3 ×/day for 30 min to provide additional nourishment for the growing biofilms (Fig. 1B). The splints were only removed during meals and the intake of drinks other than water, and when participants performed oral hygiene procedures. Outside the mouth, the splints were kept in a humid chamber to prevent dehydration of the biofilm samples. The participants documented their compliance on provided sheets. After 48 h, all biofilm carriers were collected and subjected to either pH-FISH or 16S rRNA gene sequencing (Fig. 1C).

DNA extraction, 16S rRNA gene sequencing, and analysis

Immediately after collection, one biofilm carrier from each participant was washed in phosphate-buffered saline (PBS, 10 mM, pH 7.4; Sigma–Aldrich, St. Louis, MO, USA) and stored in a PowerBead tube (Qiagen, Hilden, Germany) containing PowerBead Solution (Qiagen) at − 20 °C. DNA extraction was subsequently performed using the DNeasy PowerLyzer® PowerSoil®200 DNA Isolation Kit (Qiagen) following the manufacturer's instructions. PCR of the bacterial V3–V4 region was done using the primers Bac 314F and Bac 805R [25], followed by paired-end amplicon sequencing (2 × 300 bp) on an Illumina MiSeq sequencer using the V3 sequencing kit (Illumina, Inc., San Diego, CA, USA), as described previously [26].

Primers and barcodes were removed from the sequences using cutadapt v. 0.2.0 [27]. Error correction, amplicon sequence variant (ASV) calling, chimera removal, and taxonomic classification were performed with the R package "DADA2" v. 1.27.1 [28]. The RDP

classifier trainset number 18 of the Ribosomal RNA Database (*rrn*DB version 5.8) [29] was used for taxonomic classification and to correct for differences in the 16S rRNA gene copy number in each taxon. An rRNA gene copy number of 1 was assumed for ASV without proper classification. DNA extraction blanks and PCR negatives were used for decontamination of the data using the R package Decontam v. 1.19.0 [30]. Contaminants were identified using the prevalence method with a threshold of 0.1 and subsequently removed from the data. Rarefaction curves, plotted using the "rarecurve" function in the R package Vegan v.2.6–4 [31], showed that sufficient sequencing depth was achieved for all samples (Fig. S1). Differential abundance analysis was performed to identify differentially abundant genera between the two groups using ANCOM-BC v. 2.2.2 [32]. All sequence analyses were performed in R v. 4.3.0 [33].

Confocal microscopy-based pH ratiometry

The ratiometric pH-sensitive dye C-SNARF-4 (Thermo Fisher Scientific, Roskilde, Denmark) was used to monitor the biofilm pH response to sucrose [21] (Fig. S2). Dye calibration procedures are described in Supplemental Material 1. For ratiometric pH analysis, each glass slab was washed with 400 µL of sterile saline (0.9% NaCl, pH 7.0) and then placed on a coverslip with the biofilm facing downward in 20 µL of saline containing sucrose (4% w/v) and C-SNARF-4 (30 µM). The biofilm response to sucrose was monitored in the nine laser-marked FOVs. Images were acquired at the bottom of the biofilms after 10 min (T1) and 35 min (T2) with the same microscope settings used for dye calibration (Zeiss LSM 700; Zeiss, Jena, Germany). The experiments were performed using biological triplicates from each participant.

Biofilm fixation

Immediately after pH ratiometry, the glass slabs were gently washed with 200 µL of PBS (pH 7.4), which has been shown to remove any residual fluorescence from C-SNARF-4 [34]. The glass slabs were then transferred to ice-chilled microscopy slides with the biofilms facing up. Low melting temperature agarose (0.2% w/v UltraPure™ Agarose; Invitrogen, Carlsbad, CA, USA) was dissolved in PBS (pH 7.4) and pre-heated to 45 °C. A 9:1 (v/v) mix of the pre-heated agarose solution and 23.5% paraformaldehyde (PFA; Carl Roth, Karlsruhe, Germany) was prepared for biofilm embedding and fixation. Six microliters of the agarose-PFA mix was added to each biofilm and the glass slabs were incubated in closed chambers for 1 h at 4 °C. After fixation, the biofilms were washed by immersion in PBS (pH 7.4; 2×, 5 min each) and milli-Q water (1×, 2 min), then allowed to dry at 46 °C.

Fluorescence in situ hybridization

Prior to in situ hybridization, the embedded biofilms were dehydrated in a series of ethanol washes (25%, 50%, 75%, and 99%; 3 min each) and permeabilized with 10 µL of lysozyme mix (70 U/mL lysozyme in 100 mM Tris/HCl, pH 7.5, and 5 mM EDTA; Merck, Søborg, Denmark) for 9 min at 37 °C in a humid chamber. After washing with milli-Q water, the biofilms were hybridized in a humid dark chamber for 3 h at 46 °C using 10 µL of hybridization buffer (0.9 M NaCl, 20 mM Tris/HCl pH 7.5, 0.01% SDS, 25% formamide) containing 1 µL of each probe (10 pmol/µL, 1 pmol/µL final concentration). Double-labeled FISH probes that target all oral streptococci (STR405, labeled with ATTO488) [35], all oral *Veillonella* spp. (VEI488, labeled with ATTO550) [36], and a general bacterial probe (EUB338, labeled with ATTO633) were used for the in situ hybridizations, as detailed in Supplemental Material 1. After hybridization, all biofilms were washed in buffer (20 mM Tris/HCl pH 7.5, 5 mM EDTA, 0.01% SDS, and 215 mM NaCl) for 15 min in a water bath at 48 °C, then rinsed in ice-cold milli-Q water for 3 s. The glass slabs were subsequently placed on coverslips with the biofilm facing downward in 20 µL of a 1:4 (v/v) mix of Citifluor AF1 (Citifluor, Canterbury, UK) and VectaShield (Vector Laboratories, Newark, CA, USA) for confocal microscopy imaging (Zeiss LSM 700).

The specificity of each employed probe was checked in silico against the 16S rRNA gene sequences of the expanded Human Oral Microbiome Database (eHOMD) [37] (Fig. S3), and the absence of predicted hairpins and duplexes was checked in the software Oligo (V 7.0) [38]. Pure cultures of target and non-target organisms for each probe were fixed with PFA 4% and included as positive and negative controls in all FISH experiments (Fig. S3). Control hybridizations of in situ grown biofilms with NONEUB probes (10 pmol/µL, double-labeled with ATTO488, ATTO550, or ATTO633) (Table S2) and DAPI (4,6-diamidine-2-phenylindole; 1 µg/mL; Sigma–Aldrich) were performed to check for unspecific probe binding. Additionally, a control biofilm sample obtained from a healthy participant was subjected to pH ratiometry and FISH and subsequently imaged using SYTO41 (1 µM; Thermo Fisher Scientific, Waltham, MA, USA) between each step of the FISH procedure to monitor changes in the biofilm structure after fixation, dehydration, permeabilization, and in situ hybridization procedures. Hybridization of this sample was performed with probes EUB338 (100 ng/µL, mono-labeled with ATTO663), and STR405 (100 ng/µL, mono-labeled with ATTO488) (Fig. S4).

Confocal microscopy of in situ-hybridized biofilms

Following FISH, single-slice images of the same biofilm areas that were imaged for pH ratiometry were acquired at the bottom of the biofilms. In addition, 6-sliced z-stacks spanning the height of the biofilms in the laser-marked FOVs were obtained. Two imaging channels were used sequentially to reduce spectral bleed-through. The following excitation/detection settings were used for channel 1: STR405-ATTO488 (488 nm/300–629 nm) and EUB338-ATTO633 (639 nm/644–800 nm), and for channel 2: VEI488-ATTO550 (555 nm/560–600 nm). Images were acquired with an image size of 1440 × 1440 pixels (101.61 × 101.61 μm^2), a pixel dwell time of 1.12 μs, a pinhole size of 1.57 AU (1.3 μm optical section), and an 8-bit intensity resolution. For single-slice images, linear averaging ($n = 4$) was applied.

Digital image analysis

Extracellular biofilm pH in the ratiometric images was determined by digital image analysis, as described elsewhere [39]. Briefly, green and red channel C-SNARF-4 images were exported to the software daime (digital image analysis in microbial ecology, v. 2.2) [40] and segmented using an intensity threshold to remove the microbial cells. The fluorescence intensity ratios (green/red) in the extracellular space were calculated using the software ImageJ [41] (Fig. S5), and then converted to pH values using Eq. 1. Average pH values per FOV were calculated and used for all statistical tests.

$$pH = \left(\left(\left(\frac{2.249}{r - 0.171}\right) - 1\right) \times 136977785393\right)^{\frac{1}{14.53178}} \quad (1)$$

The total biovolumes of the microorganisms targeted with each of the probes were determined in the single-sliced and in the 6-sliced z-stack FISH images. Images were segmented by intensity thresholding in the software daime [40]. For z-stacks, the total microbial biovolumes were estimated by multiplying the respective microbial-covered areas by the interslice distance, according to the Cavalieri principle [42]. The biovolumes stained by STR405 and VEI488 were normalized to the EUB388-stained biovolumes (% total biovolume). The digital image analysis procedures are illustrated in Fig. S5. Additionally, to ensure that biovolume estimations were not biased by cell size differences between the groups, the average size of individual streptococcal and *Veillonella* spp. cells was estimated. For this, one arbitrary green and red channel image per study participant was selected and the size of 20 cells per image was measured using the software daime [40].

Statistical analysis

Differences in biofilm pH between caries-active and healthy participants at both time points (10 min and 35 min after exposure to sucrose), intra-group pH differences between time points, and differences in the relative abundance of streptococci and *Veillonella* spp. between caries-active and healthy subjects were analyzed at the FOV level using linear mixed-effects models that accounted for the clustering of different FOVs within the same biofilms and the clustering of biofilms within the same patients. The relationship between the relative abundance of streptococci and *Veillonella* spp. in each FOVs and local biofilm pH (10 min) was analyzed by a linear mixed-effects model that accounted for the clustering of FOVs, biofilms, and patients within groups. Differences in biofilm height were analyzed using paired *t*-tests after data were checked for normal distribution and homogeneity of variance using the Shapiro–Wilk and Levene tests, respectively. Statistical analyses were performed with the software R v. 4.3.0 [33] and GraphPad Prism v. 10 (GraphPad Software Inc., San Diego, CA, USA) with a significance level of $\alpha = 0.05$.

Results

All participants completed the study without deviations from the protocol (Fig. 1). Robust and dense biofilm formation was observed for both caries-active and healthy participants, with average biofilm heights of 23.2 ± 5.9 SD μm and 25.6 ± 9.8 SD μm ($P = 0.487$, $N = 9$ biofilms per group), respectively. The biofilm structure remained stable throughout all steps of the pH-FISH protocol, i.e., the C-SNARF-4 imaging, embedding/fixation, dehydration, permeabilization, and in situ hybridization of the biofilms (Fig. S4). Bacterial clusters could be re-identified in all laser-marked FOVs, while aggregates consisting of few cells and single cells were not always preserved.

Biofilm pH was significantly lower in the caries-active group at both time points ($P < 0.001$) (Fig. 2), with average pH values of 5.9 ± 0.3 SD (10 min) and 5.8 ± 0.4 SD (35 min) for healthy participants, and 5.6 ± 0.2 SD (10 min) and 5.5 ± 0.2 SD (35 min) for caries-active patients. No significant pH drop was observed between 10 and 35 min for both groups ($P = 0.66$ and 0.13, respectively). Biofilm pH varied considerably between different FOVs inside the same biofilm, with similar average variances for both groups at 10 min (healthy 0.008 ± 0.005 SD, caries-active 0.011 ± 0.002 SD) and 35 min (healthy 0.010 ± 0.008 SD, caries-active 0.010 ± 0.002 SD) of sucrose exposure. The largest pH difference observed between different FOVs inside one biofilm was 0.55 for the healthy participants and 0.51 for the caries-active patients.

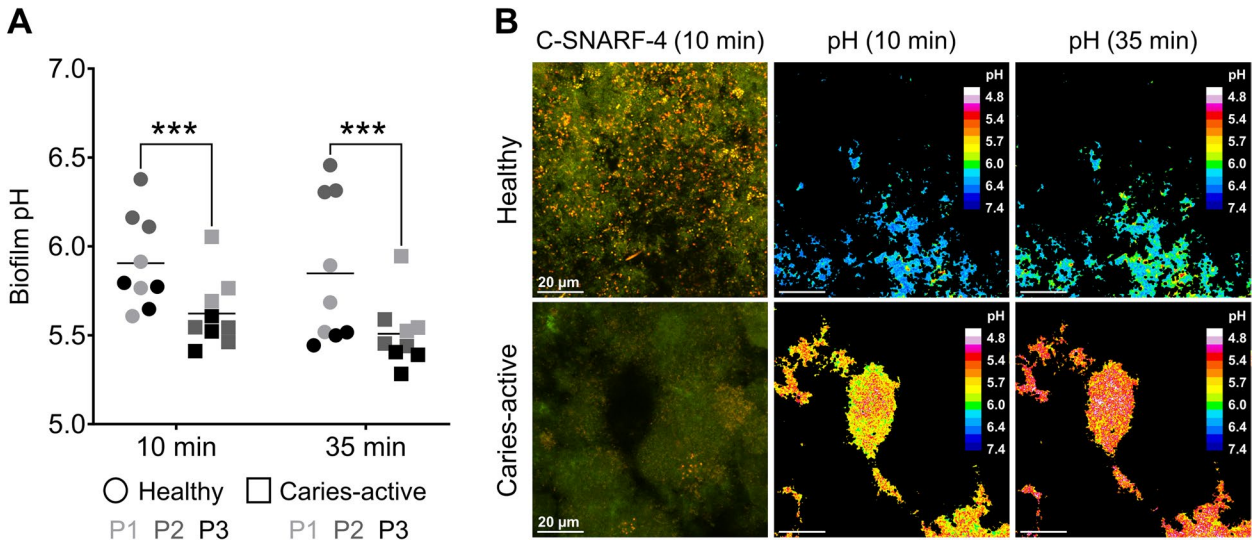

Fig. 2 Extracellular pH in biofilms collected from healthy and caries-active participants, as determined by pH ratiometry. **A** Biofilms from healthy participants exhibited a higher average extracellular pH compared to the ones obtained from caries-active patients after both 10 and 35 min of sucrose challenge (***$P < 0.001$; linear mixed-effects model). Lines = mean extracellular pH. Data from three biological replicates per participant (P1, P2, P3) per group. **B** Representative images of biofilms from a healthy (P2) and a caries-active participant (P1), stained with the ratiometric dye C-SNARF-4 (left panels). After digital image analysis, false-coloring was applied to visually illustrate the average extracellular pH after 10 min (middle panels; healthy pH 6.33, caries-active 5.74.) and 35 min (right panels; healthy pH 6.17, caries-active pH 5.53) of biofilm exposure to sucrose

The microbial biofilm composition at the genus level, as determined by 16S rRNA gene sequencing, was similar for both participant groups (Fig. 3A; Supplemental Material 2). Biofilms from healthy subjects and caries-active patients were dominated by *Streptococcus* spp. (mean relative abundances 38.6 ± 24.1% and 51.4 ± 14.9%, respectively) and *Veillonella* spp. (mean rel. abundances 12.5 ± 4.5% and 10.2 ± 2.3%, respectively), with smaller contributions from other genera. Only the genus *Fusobacterium* showed significant differences in abundance between groups ($P = 0.007$), with a higher abundance in the healthy participants (3.4 ± 2.5 vs. 0.4 ± 0.3% in caries-active patients).

Based on the sequencing results, genus-specific probes that target all oral *Streptococcus* spp. (STR405) and oral *Veillonella* spp. (VEI488) were selected for the FISH experiments. At a formamide concentration of 25% (v/v), the genus-specific probes visualized the respective target organisms, but not the negative controls; the domain bacteria probe EUB338 visualized all cells in the controls (Fig. S3). Control hybridizations with NONEUB probes showed no unspecific binding or autofluorescence in the samples (Fig. S6).

The typical arrangement of streptococci and *Veillonella* spp. in the biofilms is shown in Fig. 3B. *Veillonella* spp. predominantly appeared as single coccal cells or diplococci interspersed with streptococci in cell clusters of varying density. The average size (pixels) of individual streptococci (healthy 5.1 ± 0.1, caries-active 5.1 ± 0.3, corresponding to average diameters of 0.7 µm) and *Veillonella* spp. cells (healthy 5.9 ± 0.1, caries-active 6.0 ± 0.4, corresponding to average diameters of 0.8 µm) was similar between groups. In FISH images, streptococci were significantly more abundant in caries-active patients ($P = 0.008$), while *Veillonella* spp. were present in higher levels in healthy participants ($P < 0.001$). The relative abundance of streptococci in a FOV correlated negatively with the local pH determined after 10 min of sucrose exposure across all samples ($P = 0.03$), indicating that higher levels of streptococci were associated with lower biofilm pH areas. Within groups, the correlation reached the level of significance for caries-active patients ($P = 0.03$), but not for healthy participants ($P = 0.68$). The opposite trend, although not statistically significant, was observed for *Veillonella* spp. (all samples, $P = 0.10$; caries-active, $P = 0.08$; healthy, $P = 0.39$). Comprehensive data for pH at the FOV level and the relative abundance of streptococci and *Veillonella* spp. are shown in Fig. 4.

Discussion

Correlative analyses between microbial identity and metabolism are essential for understanding the activities of microorganisms in their natural environments [43]. FISH is a powerful tool for identifying and visualizing microorganisms within complex ecosystems [44]; however, combining the study of the spatial organization of microbial communities by FISH with the

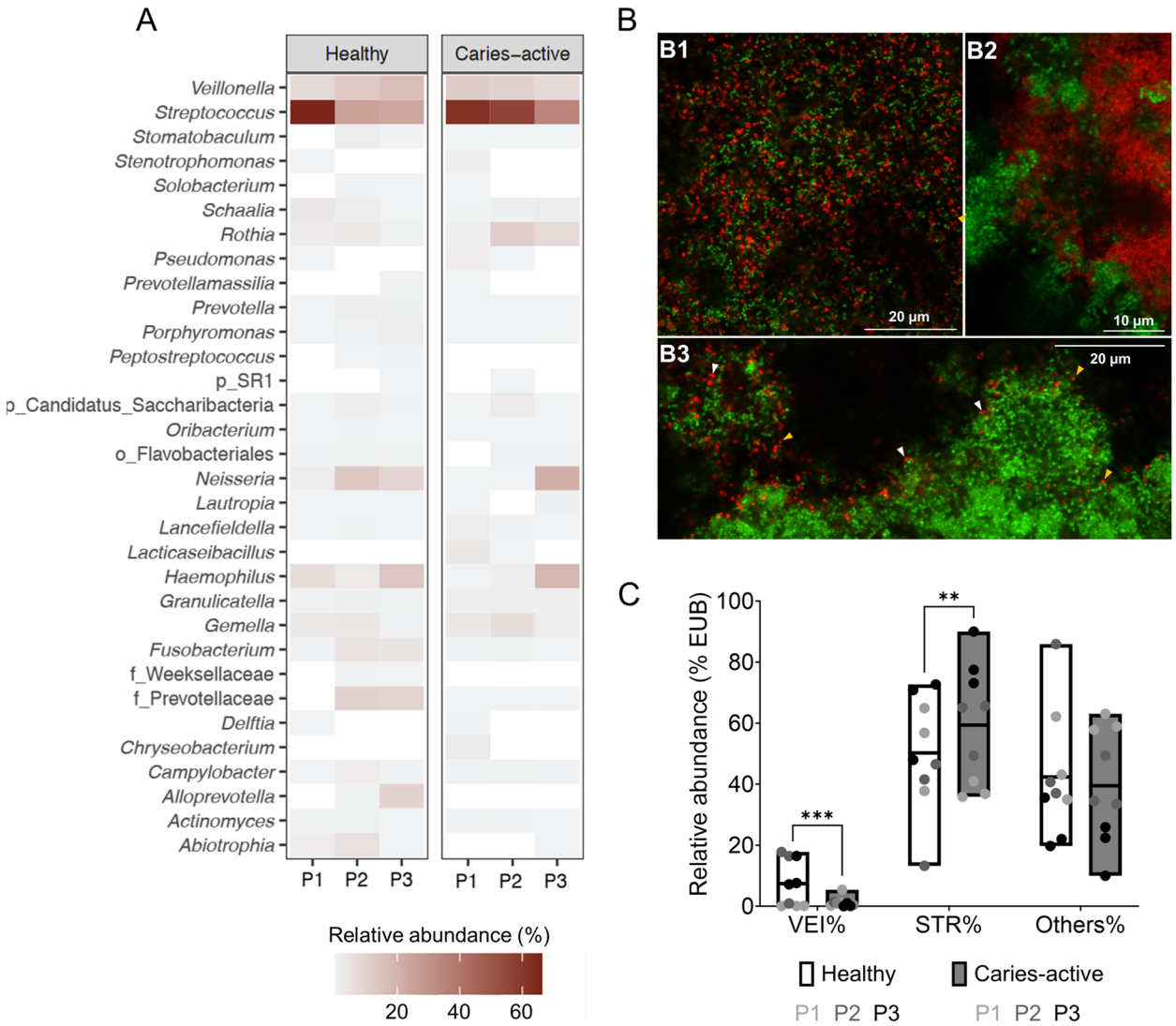

Fig. 3 Microbial composition of the biofilms collected from healthy and caries-active participants. **A** Heatmap of the relative abundance of the 32 most abundant genera (mean relative abundance above 0.2%) for each participant, determined by 16S rRNA gene amplicon sequencing for one biofilm per group ($N = 3$ participants). **B** Typical arrangement of the two most abundant genera, *Streptococcus* (green) and *Veillonella* (red), in biofilms from healthy and caries-active participants, as visualized by fluorescence in situ hybridization. Cells of both genera colocalized tightly, either spread across the biofilms (B1) or else as dense bacterial clusters (B2). In some instances, *Veillonella* spp. colonized in the periphery of streptococcal clusters (B3). White arrows, *Veillonella* spp. diplococci; yellow arrows, *Veillonella* spp. single cells. **C** The relative abundance of streptococci and *Veillonella* spp. was estimated in 6-sliced z-stacks acquired in nine laser-marked areas for each biofilm. Streptococci were significantly more abundant in caries-active patients (**$P = 0.008$), while the relative abundance of *Veillonella* spp. was significantly higher in healthy participants (***$P < 0.001$; linear mixed-effects models). Bars represent mean, maximum, and minimum values. Data from three biological replicates per participant (P1, P2, P3) per group

investigation of microbial metabolism remains a major challenge. In this study, a novel method that combines pH ratiometry with FISH (pH-FISH) was developed for the coupled investigation of microbial acid metabolism and biofilm composition at the microscale. Dental biofilms are a prime example of complex microbial communities, characterized by localized areas of low pH that may favor the development of dental caries [7, 45]. Here, we applied pH-FISH to visualize pH in dental biofilms at the microscale along with the distribution of two major genera involved in acid metabolism, namely *Streptococcus* and *Veillonella*. The biofilms were grown in situ in healthy and caries-active subjects, on carriers that mimicked the human enamel surface and allowed for the subsequent microscopy-based analysis of structurally preserved biofilms.

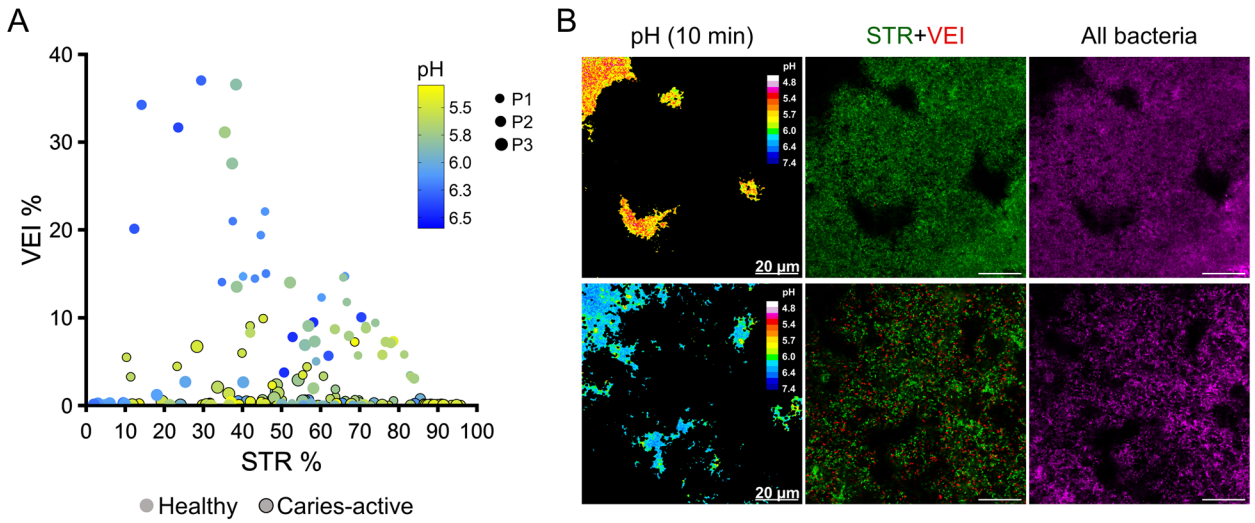

Fig. 4 Relationship between local biofilm composition and pH. **A** Relative abundance of streptococci (STR %) and *Veillonella* spp. (VEI %) observed at the field of view (FOV) level for healthy and caries-active participants, plotted against the respective local biofilm pH measured after 10 min of sucrose challenge. Low pH areas correlated with a higher abundance of streptococci ($P = 0.03$); an opposite trend was observed for *Veillonella* spp., but it did not reach statistical significance ($P = 0.10$). Linear mixed-effects models with a significance level of $\alpha = 0.05$. Data from three biological replicates per participant (P1, P2, P3) per group. **B** Representative images show the local biofilm pH in a FOV dominated by streptococci (upper panels; mean pH 5.72) and in a FOV with high levels of *Veillonella* spp. (lower panels; mean pH 6.23)

Streptococcus spp. are potent producers of organic acids, primarily lactic acid, from dietary carbohydrates and are well recognized for their role in caries development [10, 46]. The non-saccharolytic *Veillonella* spp., in contrast, are able to utilize lactate as a carbon and energy source. They have been associated with the occurrence of periodontal disease, but in the context of dental caries, their metabolic activity may mitigate the pH drops caused by other organisms [47]. Data from epidemiological studies have consistently associated increased levels of streptococci with dental caries [48–50]. For *Veillonella* spp., however, data from association studies are less consistent. Some investigations have linked a high prevalence/abundance of *Veillonella* spp. to health [48] and some to disease [49, 51, 52]. In our study, biofilm pH, as measured by pH ratiometry, was significantly lower in biofilms from caries-active patients, which also exhibited a higher relative abundance of streptococci. In contrast, *Veillonella* spp. were more abundant in biofilms from healthy participants. Interestingly, the relative abundance of streptococci correlated negatively with biofilm pH at the FOV level across all samples, and also within samples from caries-active patients; an opposite trend, although not significant, was observed for *Veillonella* spp. These findings suggest that clusters of streptococci impact the local pH and may contribute to the formation of acidic pockets inside the biofilms. *Veillonella* spp., on the other hand, seem to have a protective role against biofilm acidification [47]. Their elevated prevalence in some epidemiological studies on diseased populations may, therefore, be explained by the increased production of lactate in cariogenic biofilms, which favors the growth of lactate-catabolizing species [46–48]. Taken together, these findings demonstrate the importance of spatially resolved analyses of biofilm community composition and metabolism.

Combining chemical imaging of key metabolites and structural imaging of the biofilm microarchitecture has the potential to unravel important links between biofilm structure, community composition, and virulence. Recently, Kim et al. (2020) have elegantly demonstrated in a simplified two-species model that rotund-shaped clusters of *Streptococcus mutans* are associated with microscale foci of enamel demineralization, and hence the onset and progression of dental caries [9]. pH-FISH allows for the combined analysis of biofilm architecture, community composition, and metabolism, not only in well-defined model systems, but also in complex in vivo-grown microbial communities. Thereby, it has the potential to provide insights into fundamental biological processes, such as those related to pathogenic mechanisms, within natural microbial systems.

Dental biofilms are highly complex microbial communities with an intimate link between biofilm pH and virulence, but pH is also a key determinant for biofilm metabolism in many other biological systems. Local changes in biofilm pH affect the output of industrial fungal fermentation [53], as well as the electricity generation

in microbial fuel cells [54] and the activity and growth of nitrifying bacteria [55, 56]. In the medical field, the pH of wound infections can support or reduce the rate of microbial proliferation and wound healing [57]. Similarly, pH drops in the lung milieu can favor the establishment of bacterial infections in cystic fibrosis patients [58, 59]. Changes in biofilm pH can be accurately monitored in a spatial- and time-resolved fashion by pH ratiometry [21, 22], while FISH with taxa-specific probes enables the identification and visualization of the spatial distribution of relevant microbial groups within these microbial communities [60].

The preservation of the three-dimensional biofilm architecture is crucially important for correlative imaging during pH-FISH. pH ratiometry needs to be performed on fresh, metabolically active biofilms [61], while conventional FISH requires the fixation and permeabilization of the samples [60]. To accommodate both requirements, pH ratiometry has to be performed prior to sample preparation for FISH, and the standard fixation procedure had to be optimized considerably to ensure preservation of the native biofilm structure. Embedding the biofilm in a gel matrix (agarose) to provide physical support and stabilization during PFA fixation, reducing the mechanical stress caused by cross-linking, proved to be an efficient method for biofilm preservation (Fig. S4). Throughout the whole series of processing steps, samples needed to be handled with great care to minimize shear stress to the biofilms, especially during washing procedures. It is conceivable that, without further adaptations, pH-FISH cannot be performed successfully on biofilms that are less robust than in vivo-grown dental biofilms, e.g., laboratory model biofilms that are not exposed to shear during growth.

pH-FISH is also limited by the penetration depth of confocal microscopy [62], and by the taxonomic resolution of oligonucleotide probes. In this study, sequencing and FISH analyses were limited to genus level resolution, and therefore, associations between distinct streptococcal (or *Veillonella*) species and biofilm pH were not addressed. Future work may use FISH probes with higher taxonomic resolution, as well as methods to increase the number of detectable targets (e.g., Combinatorial Labeling and Spectral Imaging-FISH; CLASI-FISH) [63]. While we used the dye C-SNARF-4 for pH ratiometry, which has a dynamic range between pH 4.5 and 7.0, the method may be adapted to other pH-sensitive, ratiometric dyes that are suitable for alkaline (e.g., C-SNARF-1) or more acidic (e.g., Oregon green) conditions [23]. This study only measured horizontal pH profiles at the biofilm base, but in principle, pH-FISH can be employed to correlate both horizontal and vertical pH gradients to biofilm composition [22]. Biofilms were collected on glass slabs, but pH-FISH can likely be extended to other carrier materials, as both pH ratiometry and FISH have been successfully performed on biofilms grown on hydroxyapatite discs, enamel specimens, polymeric restorative materials, and titanium and zirconia surfaces [64–67]. However, further optimization may be required to avoid interference of autofluorescent substrates on pH-FISH images.

Conclusion

In summary, pH-FISH allows for the combined imaging of biofilm pH and microbial biofilm architecture. As a proof-of-concept, we applied the method to dental biofilms and demonstrated that a high local abundance of *Streptococcus* spp. correlates with a lower pH. pH-FISH thus represents a powerful method to explore the complex interplay between biofilm structure and metabolism at the microscale, with potential applicability in various other biological systems.

Abbreviations

ASV	Amplicon sequence variant
FISH	Fluorescence in situ hybridization
FOV	Field of view
PBS	Phosphate-buffered saline
PFA	Paraformaldehyde
pH-FISH	pPH ratiometry combined with fluorescence in situ hybridization

Supplementary Information

The online version contains supplementary material available at https://doi.org/10.1186/s40168-024-01977-9.

Supplementary Material 1.

Supplementary Material 2.

Supplementary Material 3.

Acknowledgements

This study was supported by the Faculty of Health, Aarhus University, Denmark. The authors would like to thank Dimitra Sakoula, Nicole Geerlings, Holger Daims, Sarah Al-Ajeel, Eero Juhani Raittio, Burak Avci, and Mario Vianna Vettore for fruitful discussions. Lisbeth Ann Abildtrup, Anette Aakjær Thomsen, and Dirk Leonhardt are acknowledged for the excellent technical assistance. We thank Pernille Dukanovic Rikvold, Mathilde Frost Kristensen, and Sahar Assar for the clinical support.

Authors' contributions

Y.C.D.R.: conceptualization, methodology, data acquisition, formal analysis, investigation, visualization, writing – original draft; K.K.: methodology, writing – review and editing; M.B.L.: formal analysis, visualization, writing – review and editing; A.S.: conceptualization, supervision, resources, writing – review and editing; R.L.M.: supervision, resources, writing – review and editing; MW: resources, writing – review and editing; S.S.: conceptualization, methodology, formal analysis, supervision, writing – original draft, writing – review and editing.

Funding

This study did not receive any specific funding. KK and MW acknowledge funding from the Austrian Science Fund (FWF) for the Cluster of Excellence "Microbiomes drive Planetary Health" (doi.org.1055776/COE7). For open access purposes, the authors have applied a CC BY public copyright license to any author accepted manuscript version arising from this submission.

Data availability
The data generated during this study are available within the article and its Additional files. Sequence files and metadata for all samples are also publicly available under the Bioproject ID PRJNA1118491.

Declarations

Ethics approval and consent to participate
The study was approved by the Ethical Committee of Region Midtjylland (case no. 1–10-72–178-18). Written informed consent was obtained from all study participants.

Consent for publication
Not applicable.

Competing interests
The authors declare no competing interests.

Received: 6 July 2024 Accepted: 12 November 2024
Published online: 20 December 2024

References

1. Amann RI, Ludwig W, Schleifer KH. Phylogenetic identification and in situ detection of individual microbial cells without cultivation. Microbiol Rev. 1995;59:143–69. https://doi.org/10.1128/mr.59.1.143-169.1995.
2. Wilbert SA, Mark Welch JL, Borisy GG. Spatial ecology of the human tongue dorsum microbiome. Cell Rep. 2020;30:4003-4015.e3. https://doi.org/10.1016/j.celrep.2020.02.097.
3. Gieseke A, Bjerrum L, Wagner M, Amann R. Structure and activity of multiple nitrifying bacterial populations co-existing in a biofilm. Environ Microbiol. 2003;5:355–69. https://doi.org/10.1046/j.1462-2920.2003.00423.x.
4. Moter A, Leist G, Rudolph R, Schrank K, Choi BK, Wagner M, G Bel UB. Fluorescence in situ hybridization shows spatial distribution of as yet uncultured treponemes in biopsies from digital dermatitis lesions. Microbiology (Reading). 1998;144(Pt 9):2459–67. https://doi.org/10.1099/00221287-144-9-2459.
5. Morillo-Lopez V, Sjaarda A, Islam I, Borisy GG, Mark Welch JL. Corncob structures in dental plaque reveal microhabitat taxon specificity. Microbiome. 2022;10:145. https://doi.org/10.1186/s40168-022-01323-x.
6. Koo H, Yamada KM. Dynamic cell-matrix interactions modulate microbial biofilm and tissue 3D microenvironments. Curr Opin Cell Biol. 2016;42:102–12. https://doi.org/10.1016/j.ceb.2016.05.005.
7. Hwang G, Liu Y, Kim D, Sun V, Aviles-Reyes A, Kajfasz JK, et al. Simultaneous spatiotemporal mapping of in situ pH and bacterial activity within an intact 3D microcolony structure. Sci Rep. 2016;6:32841. https://doi.org/10.1038/srep32841.
8. Kristensen MF, Lund MB, Schramm A, Lau EF, Schlafer S. Determinants of microscale pH in in situ grown dental biofilms. J Dent Res. 2023;102:1348–55. https://doi.org/10.1177/00220345231190563.
9. Kim D, Barraza JP, Arthur RA, Hara A, Lewis K, Liu Y, et al. Spatial mapping of polymicrobial communities reveals a precise biogeography associated with human dental caries. Proc Natl Acad Sci U S A. 2020;117:12375–86. https://doi.org/10.1073/pnas.1919099117.
10. Takahashi N, Nyvad B. Caries ecology revisited: microbial dynamics and the caries process. Caries Res. 2008;42:409–18. https://doi.org/10.1159/000159604.
11. Lee N, Nielsen PH, Andreasen KH, Juretschko S, Nielsen JL, Schleifer KH, Wagner M. Combination of fluorescent in situ hybridization and microautoradiography-a new tool for structure-function analyses in microbial ecology. Appl Environ Microbiol. 1999;65:1289–97. https://doi.org/10.1128/AEM.65.3.1289-1297.1999.
12. Li T, Wu T-D, Mazéas L, Toffin L, Guerquin-Kern J-L, Leblon G, Bouchez T. Simultaneous analysis of microbial identity and function using NanoSIMS. Environ Microbiol. 2008;10:580–8. https://doi.org/10.1111/j.1462-2920.2007.01478.x.
13. Orphan VJ, House CH, Hinrichs KU, McKeegan KD, DeLong EF. Methane-consuming archaea revealed by directly coupled isotopic and phylogenetic analysis. Science. 2001;293:484–7. https://doi.org/10.1126/science.1061338.
14. Huang WE, Stoecker K, Griffiths R, Newbold L, Daims H, Whiteley AS, Wagner M. Raman-FISH: combining stable-isotope Raman spectroscopy and fluorescence in situ hybridization for the single cell analysis of identity and function. Environ Microbiol. 2007;9:1878–89. https://doi.org/10.1111/j.1462-2920.2007.01352.x.
15. Berry D, Mader E, Lee TK, Woebken D, Wang Y, Zhu D, et al. Tracking heavy water (D2O) incorporation for identifying and sorting active microbial cells. Proc Natl Acad Sci U S A. 2015;112:E194-203. https://doi.org/10.1073/pnas.1420406112.
16. Ge X, Pereira FC, Mitteregger M, Berry D, Zhang M, Hausmann B, et al. SRS-FISH: A high-throughput platform linking microbiome metabolism to identity at the single-cell level. Proc Natl Acad Sci U S A. 2022;119:e2203519119. https://doi.org/10.1073/pnas.2203519119.
17. Ramsing NB, Kühl M, Jørgensen BB. Distribution of sulfate-reducing bacteria, O2, and H2S in photosynthetic biofilms determined by oligonucleotide probes and microelectrodes. Appl Environ Microbiol. 1993;59:3840–9. https://doi.org/10.1128/aem.59.11.3840-3849.1993.
18. Schramm A, de Beer D, Wagner M, Amann R. Identification and activities in situ of Nitrosospira and Nitrospira spp. as dominant populations in a nitrifying fluidized bed reactor. Appl Environ Microbiol. 1998;64:3480–5. https://doi.org/10.1128/AEM.64.9.3480-3485.1998.
19. Schramm A, Larsen LH, Revsbech NP, Ramsing NB, Amann R, Schleifer KH. Structure and function of a nitrifying biofilm as determined by in situ hybridization and the use of microelectrodes. Appl Environ Microbiol. 1996;62:4641–7. https://doi.org/10.1128/aem.62.12.4641-4647.1996.
20. Beyenal H, Babauta J. Microsensors and microscale gradients in biofilms. Adv Biochem Eng Biotechnol. 2014;146:235–56. https://doi.org/10.1007/10_2013_247.
21. Schlafer S, Garcia JE, Greve M, Raarup MK, Nyvad B, Dige I. Ratiometric imaging of extracellular pH in bacterial biofilms with C-SNARF-4. Appl Environ Microbiol. 2015;81:1267–73. https://doi.org/10.1128/AEM.02831-14.
22. Schlafer S, Baelum V, Dige I. Improved pH-ratiometry for the three-dimensional mapping of pH microenvironments in biofilms under flow conditions. J Microbiol Methods. 2018;152:194–200. https://doi.org/10.1016/j.mimet.2018.08.007.
23. Grillo-Hill BK, Webb BA, Barber DL. Ratiometric imaging of pH probes. Methods Cell Biol. 2014;123:429–48. https://doi.org/10.1016/B978-0-12-420138-5.00023-9.
24. Rikvold PT, Kambourakis Johnsen K, Leonhardt D, Møllebjerg A, Nielsen SM, Skov Hansen LB, et al. A new device for in situ dental biofilm collection additively manufactured by direct metal laser sintering and vat photopolymerization. 3D Printing and Additive Manufacturing 2022. https://doi.org/10.1089/3dp.2022.0009.
25. Herlemann DP, Labrenz M, Jürgens K, Bertilsson S, Waniek JJ, Andersson AF. Transitions in bacterial communities along the 2000 km salinity gradient of the Baltic Sea. ISME J. 2011;5:1571–9. https://doi.org/10.1038/ismej.2011.41.
26. Tawakoli PN, Neu TR, Busck MM, Kuhlicke U, Schramm A, Attin T, et al. Visualizing the dental biofilm matrix by means of fluorescence lectin-binding analysis. J Oral Microbiol. 2017;9:1345581. https://doi.org/10.1080/20002297.2017.1345581.
27. Martin M. Cutadapt removes adapter sequences from high-throughput sequencing reads. EMBnet j. 2011;17:10. https://doi.org/10.14806/ej.17.1.200.
28. Callahan BJ, McMurdie PJ, Rosen MJ, Han AW, Johnson AJA, Holmes SP. DADA2: High-resolution sample inference from Illumina amplicon data. Nat Methods. 2016;13:581–3. https://doi.org/10.1038/nmeth.3869.
29. Stoddard SF, Smith BJ, Hein R, Roller BRK, Schmidt TM. rrnDB: improved tools for interpreting rRNA gene abundance in bacteria and archaea and a new foundation for future development. Nucleic Acids Res. 2015;43:D593–8. https://doi.org/10.1093/nar/gku1201.
30. Davis NM, Proctor DM, Holmes SP, Relman DA, Callahan BJ. Simple statistical identification and removal of contaminant sequences in marker-gene and metagenomics data. Microbiome. 2018;6:226. https://doi.org/10.1186/s40168-018-0605-2.

31. Oksanen J, Simpson GL, Blanchet G, Kindt R, Legendre P, Minchin PR, O'Hara RB, Solymos P, MHH Stevens, Szoecs E, Szoecs E, Wagner H, Barbour M, Bedward M, Bolker B, Borcard D, Carvalho G, Chirico M, De Caceres M, Durand S, Evangelista HBA, FitzJohn R, Friendly M, Furneaux B, Hannigan G, Hill MO, Lahti L, McGlinn D, Ouellette MH, Cunha ER, Smith T, Stier A, Ter Braak CJF, Weedon J. vegan: community ecology package (R. package); 2024. https://CRAN.R-project.org/package=vegan.
32. Lin H, Peddada SD. Analysis of compositions of microbiomes with bias correction. Nat Commun. 2020;11:3514. https://doi.org/10.1038/s41467-020-17041-7.
33. R Core Team. R: a language and environment for statistical computing. R Foundation for Statistical Computing, Vienna, Austria; 2023. https://www.R-project.org.
34 Del Rey YC, Schramm A, L Meyer R, Lund MB, Schlafer S. Combined pH ratiometry and fluorescence lectin-binding analysis (pH-FLBA) for microscopy-based analyses of biofilm pH and matrix carbohydrates. Appl Environ Microbiol. 2024;90:e0200723. https://doi.org/10.1128/aem.02007-23.
35. Paster BJ, Bartoszyk IM, Dewhirst FE. Identification of oral streptococci using PCR-based, reverse-capture, checkerboard hybridization. Methods Cell Sci. 1998;20:223–31. https://doi.org/10.1023/A:1009715710555.
36 Chalmers NI, Palmer RJ, Cisar JO, Kolenbrander PE. Characterization of a Streptococcus sp.-Veillonella sp. community micromanipulated from dental plaque. J Bacteriol. 2008;190:8145–54. https://doi.org/10.1128/jb.00983-08.
37. Escapa IF, Chen T, Huang Y, Gajare P, Dewhirst FE, Lemon KP. New insights into human nostril microbiome from the expanded Human Oral Microbiome Database (eHOMD): a resource for the microbiome of the human aerodigestive tract. mSystems 2018. https://doi.org/10.1128/mSystems.00187-18.
38. Rychlik W. OLIGO 7 primer analysis software. Methods Mol Biol. 2007;402:35–60. https://doi.org/10.1007/978-1-59745-528-2_2.
39. Schlafer S, Dige I. Ratiometric imaging of extracellular pH in dental biofilms. J Vis Exp. 2016. https://doi.org/10.3791/53622.
40. Daims H, Lücker S, Wagner M. daime, a novel image analysis program for microbial ecology and biofilm research. Environ Microbiol. 2006;8:200–13. https://doi.org/10.1111/j.1462-2920.2005.00880.x.
41. Schneider CA, Rasband WS, Eliceiri KW. NIH Image to ImageJ: 25 years of image analysis. Nat Methods. 2012;9:671–5. https://doi.org/10.1038/nmeth.2089.
42. Gundersen HJ, Jensen EB. The efficiency of systematic sampling in stereology and its prediction. J Microsc. 1987;147:229–63. https://doi.org/10.1111/j.1365-2818.1987.tb02837.x.
43. Weisener CG, Reid T. Combined imaging and molecular techniques for evaluating microbial function and composition: a review. Surf Interface Anal. 2017;49:1416–21. https://doi.org/10.1002/sia.6317.
44. Amann R, Fuchs BM, Behrens S. The identification of microorganisms by fluorescence in situ hybridisation. Curr Opin Biotechnol. 2001;12:231–6. https://doi.org/10.1016/S0958-1669(00)00204-4.
45. Dige I, Baelum V, Nyvad B, Schlafer S. Monitoring of extracellular pH in young dental biofilms grown in vivo in the presence and absence of sucrose. J Oral Microbiol. 2016;8:30390. https://doi.org/10.3402/jom.v8.30390.
46. Lemos JA, Palmer SR, Zeng L, Wen ZT, Kajfasz JK, Freires IA, et al. The biology of Streptococcus mutans. Microbiol Spectr. 2019. https://doi.org/10.1128/microbiolspec.GPP3-0051-2018.
47. Zhou P, Manoil D, Belibasakis GN, Kotsakis GA. Veillonellae: beyond bridging species in oral biofilm ecology. Front Oral Health. 2021;2:774115. https://doi.org/10.3389/froh.2021.774115.
48. Grier A, Myers JA, O'Connor TG, Quivey RG, Gill SR, Kopycka-Kedzierawski DT. Oral microbiota composition predicts early childhood caries onset. J Dent Res. 2021;100:599–607. https://doi.org/10.1177/0022034520979926.
49. Ling Z, Kong J, Jia P, Wei C, Wang Y, Pan Z, et al. Analysis of oral microbiota in children with dental caries by PCR-DGGE and barcoded pyrosequencing. Microb Ecol. 2010;60:677–90. https://doi.org/10.1007/s00248-010-9712-8.
50. Winter GB. Epidemiology of dental caries. Arch Oral Biol. 1990;35(Suppl):1S-7S. https://doi.org/10.1016/0003-9969(90)90124-S.
51. Becker MR, Paster BJ, Leys EJ, Moeschberger ML, Kenyon SG, Galvin JL, et al. Molecular analysis of bacterial species associated with childhood caries. J Clin Microbiol. 2002;40:1001–9. https://doi.org/10.1128/JCM.40.3.1001-1009.2002.
52. Gross EL, Beall CJ, Kutsch SR, Firestone ND, Leys EJ, Griffen AL. Beyond Streptococcus mutans: dental caries onset linked to multiple species by 16S rRNA community analysis. PLoS ONE. 2012;7:e47722. https://doi.org/10.1371/journal.pone.0047722.
53. Mohd Azhar SH, Abdulla R, Jambo SA, Marbawi H, Gansau JA, Mohd Faik AA, Rodrigues KF. Yeasts in sustainable bioethanol production: a review. Biochem Biophys Rep. 2017;10:52–61. https://doi.org/10.1016/j.bbrep.2017.03.003.
54. Oliveira VB, Simões M, Melo LF, Pinto A. Overview on the developments of microbial fuel cells. Biochem Eng J. 2013;73:53–64. https://doi.org/10.1016/j.bej.2013.01.012.
55. Wicaksono DP, Washio J, Abiko Y, Domon H, Takahashi N. Nitrite production from nitrate and its link with lactate metabolism in oral Veillonella spp. Appl Environ Microbiol. 2020. https://doi.org/10.1128/AEM.01255-20.
56. Gieseke A, Tarre S, Green M, de Beer D. Nitrification in a biofilm at low pH values: role of in situ microenvironments and acid tolerance. Appl Environ Microbiol. 2006;72:4283–92. https://doi.org/10.1128/AEM.00241-06.
57. Percival SL, McCarty S, Hunt JA, Woods EJ. The effects of pH on wound healing, biofilms, and antimicrobial efficacy. Wound Repair Regen. 2014;22:174–86. https://doi.org/10.1111/wrr.12125.
58. Massip-Copiz MM, Santa-Coloma TA. Extracellular pH and lung infections in cystic fibrosis. Eur J Cell Biol. 2018;97:402–10. https://doi.org/10.1016/j.ejcb.2018.06.001.
59. Lin Q, Pilewski JM, Di YP. Cystic fibrosis acidic microenvironment determines antibiotic susceptibility and biofilm formation of Pseudomonas aeruginosa; 2020.
60. Pernthaler J, Glöckner F-O, Schönhuber W, Amann R. Fluorescence in situ hybridization (FISH) with rRNA-targeted oligonucleotide probes. In: Marine Microbiology: Elsevier; 2001. p. 207–226. https://doi.org/10.1016/S0580-9517(01)30046-6.
61. Hunter RC, Beveridge TJ. Application of a pH-sensitive fluoroprobe (C-SNARF-4) for pH microenvironment analysis in Pseudomonas aeruginosa biofilms. Appl Environ Microbiol. 2005;71:2501–10. https://doi.org/10.1128/AEM.71.5.2501-2510.2005.
62. Jonkman J, Brown CM, Wright GD, Anderson KI, North AJ. Tutorial: guidance for quantitative confocal microscopy. Nat Protoc. 2020;15:1585–611. https://doi.org/10.1038/s41596-020-0313-9.
63. Valm AM, Welch JLM, Rieken CW, Hasegawa Y, Sogin ML, Oldenbourg R, et al. Systems-level analysis of microbial community organization through combinatorial labeling and spectral imaging. Proc Natl Acad Sci U S A. 2011;108:4152–7. https://doi.org/10.1073/pnas.1101134108.
64. Schlafer S, Bornmann T, Paris S, Göstemeyer G. The impact of glass ionomer cement and composite resin on microscale pH in cariogenic biofilms and demineralization of dental tissues. Dent Mater. 2021;37:1576–83. https://doi.org/10.1016/j.dental.2021.08.007.
65. Dige I, Grønkjær L, Nyvad B. Molecular studies of the structural ecology of natural occlusal caries. Caries Res. 2014;48:451–60. https://doi.org/10.1159/000357920.
66. Fröjd V, de ChávezPaz L, Andersson M, Wennerberg A, Davies JR, Svensäter G. In situ analysis of multispecies biofilm formation on customized titanium surfaces. Mol Oral Microbiol. 2011;26:241–52. https://doi.org/10.1111/j.2041-1014.2011.00610.x.
67. Al-Ahmad A, Wiedmann-Al-Ahmad M, Fackler A, Follo M, Hellwig E, Bächle M, et al. In vivo study of the initial bacterial adhesion on different implant materials. Arch Oral Biol. 2013;58:1139–47. https://doi.org/10.1016/j.archoralbio.2013.04.011.

Publisher's Note